Journal of Solid State Chemistry 182 (2009) 1545–1549

Contents lists available at ScienceDirect

Journal of Solid State Chemistry

journal homepage: www.elsevier.com/locate/jssc

High-pressure structural behavior and equation of state of $NaZnF_3$

Sergey Yakovlev [a,*], Maxim Avdeev [a], Mohamed Mezouar [b]

[a] Bragg Institute, Australian Nuclear Science and Technology Organisation, 1 PBM, Menai, NSW 2234, Australia
[b] ID-27, European Synchrotron Radiation Facility (ESRF), 6 rue Jules Horowitz, PB220, 38043 Grenoble CEDEX, France

ARTICLE INFO

Article history:
Received 13 January 2009
Received in revised form
22 March 2009
Accepted 29 March 2009
Available online 7 April 2009

Keywords:
Perovskite
Postperovskite
Pressure
Diamond anvil cell
Synchrotron X-ray diffraction
Rietveld refinement
Ab-initio calculation

ABSTRACT

We report the results of density functional theory ab-initio calculations and monochromatic synchrotron X-ray diffraction study carried out for orthorhombic $NaZnF_3$ in the pressure range 0–40 GPa. Perovskite-to-postperovskite phase transition was anticipated by first-principles computations and then observed in high-pressure diamond anvil cell synchrotron diffraction experiment between 14 and 22 GPa. Above 25 GPa postperovskite structure ($CaIrO_3$ type, space group *Cmcm*) coexists with another phase, yet unidentified. On decompression, pure postperovskite-type structure was found to be stable down to 4 GPa; below this pressure sample contained both perovskite and postperovskite modifications. Fit of experimental *P–V* data to the third-order Birch–Murnaghan equation of state gave bulk moduli, K_{P0} 64.98 ± 2.67 and 69.88 ± 3.69 GPa for perovskite and postperovskite modifications, respectively. Both phases demonstrated strong anisotropy of compressibility. For postperovskite $NaZnF_3$, the highest compression was observed along the direction perpendicular to the planes of ZnF_6 octahedra arrangement.

1. Introduction

Perovskites represent the most distributed group of minerals. Furthermore, many materials of this structural type possess technologically attractive properties (ferroelectricity, magnetism, ionic conductivity, etc.) [1]. For earth science, perovskites are of particular importance due to recently observed pressure-induced perovskite (pv)-to-postperovskite (ppv) ($CaIrO_3$-type) phase transitions in $MgSiO_3$ [2,3], $MnGeO_3$ [4], $MgGeO_3$ [5] and $NaMgF_3$ [6]. It is believed that this transition is responsible for D'' seismic discontinuity at Earth lower mantle-core boundary. These observations aroused significant interest to high-pressure crystal chemistry of perovskites. Last years progress in diamond anvil cell (DAC) technique development considerably facilitated data acquisition and made high-pressure structural study routine [7,8].

Recently, we reported the results of systematic study of crystallographic data of about 1300 perovskites from the Inorganic Crystal Structucture Database (ICSD)[1] [9]. This analysis let us, in particular, to outline the group of compounds in which transition to postperovskite structure may potentially be observed in the experimentally achievable pressure range.

In this report, we present the results of first-principles density functional theory (DFT) calculations and high-pressure synchrotron X-ray diffraction study of $NaZnF_3$. This fluorite perovskite belongs to *Pnma* orthorhombic space group and is characterized by high degree of distortion expressed in terms of polyhedral volume ratio (V_A/V_B) [9]. For $NaZnF_3$ V_A/V_B is equal to 4.28 ($V_A/V_B = 5$ for the ideal cubic structure). We demonstrate that, according to ab-initio computer simulations, postperovskite $CaIrO_3$-type modification of $NaZnF_3$ becomes more stable (relative to perovskite) above 25.4 GPa. In high-pressure synchrotron X-ray diffraction experiment, gradual perovskite-to-postperovskite phase transformation was observed in the pressure range from 14 to 22 GPa. Above 25 GPa, additional features in X-ray spectra inconsistent with $CaIrO_3$ structural model appear presumably indicating another phase transition to high-pressure kinked polymorph of postperovskite. Perovskite-to-postperovskite phase is found to be irreversible: on decompression, pure postperovskite phase is preserved to the pressure as low as 4 GPa.

2. Experimental methods and computational procedure

The powder of $NaZnF_3$ was prepared via a conventional solid-state synthesis route from NaF and ZnF_2. Equimolar mixture of starting fluorides was pressed and annealed in a tube furnace in flowing dry Ar (5.0) at 635 °C for 24 h in presence of Cu pieces. Ar was additionally dried with silica gel. Phase composition of the sample was analyzed by X-ray diffraction. The sample was found

* Corresponding author. Present address: University of Twente, Faculty of Science and Technology, Inorganic Membranes, PO Box 217, 7500 AE Enschede, The Netherlands.
E-mail address: s.yakovlev@tnw.utwente.nl (S. Yakovlev).

[1] Inorganic Crystal Structure Database, ICSD (2007), http://www.fiz-karlsruhe.de/icsd.html

0022-4596/$ - see front matter © 2009 Elsevier Inc. All rights reserved.
doi:10.1016/j.jssc.2009.03.031

to consist of perovskite $NaZnF_3$ as a main phase. We also detected inclusion of ZnO. Processing conditions were carefully adjusted to minimize oxidation of Zn. It was, however, not possible to obtain single phase sample by the described method. We found later that ZnO did not contribute to a noticeable extent to synchrotron X-ray diffraction data.

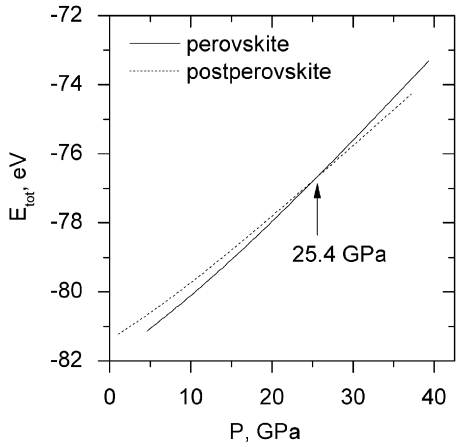

Fig. 1. Pressure-dependent total energies of perovskite (pv) and postperovskite (ppv) unit cells obtained from DFT ab-initio computation.

High pressure X-ray diffraction experiments were conducted at the European Synchrotron Radiation Facility (ESRF, beamline ID 27, $\lambda = 0.3738$ Å). Isostatic pressure up to 40 GPa was applied using gas-driven diamond anvil cell with stainless steel gasket and Ne as a pressure transmitting medium. Few grains of ruby were loaded to the cell and pressure at the sample was controlled by fluorescence method [10]. Detailed description of the experimental technique can be found elsewhere [7]. Data from image plate were integrated using FIT2D software [11]. EXPGUI front-end [12] for GSAS program [13] was used for Rietveld refinement.

First-principles calculations of the total energies of perovskite and postperovskite modifications of $NaZnF_3$ were performed on the Australian Partnership for Advanced Computing (APAC) National Facility (Canberra). Calculations were carried out within the generalized gradient approximation implemented in VASP (Vienna Ab-initio Simulation Package) code (see [14] and references therein for more details) for a wide pressure range. Brillouin zone integrations were done using Monkhorst–Pack meshes of **k**-points: $3 \times 3 \times 2$ and $5 \times 2 \times 3$ for perovskite and postperovskite cells, respectively. Parameters were selected to preserve near cubic supercells in a reciprocal space. Cut off energy was fixed at 400 eV for all calculations. During energy minimization, the cell volume was kept fixed (at certain P) while ionic coordinates and cell shape were allowed to vary. Structural optimization was performed for each pressure value. In the case of postperovskite phase, fractional coordinates of $CaIrO_3$ (space group *Cmcm*) were used to build an initial structural model.

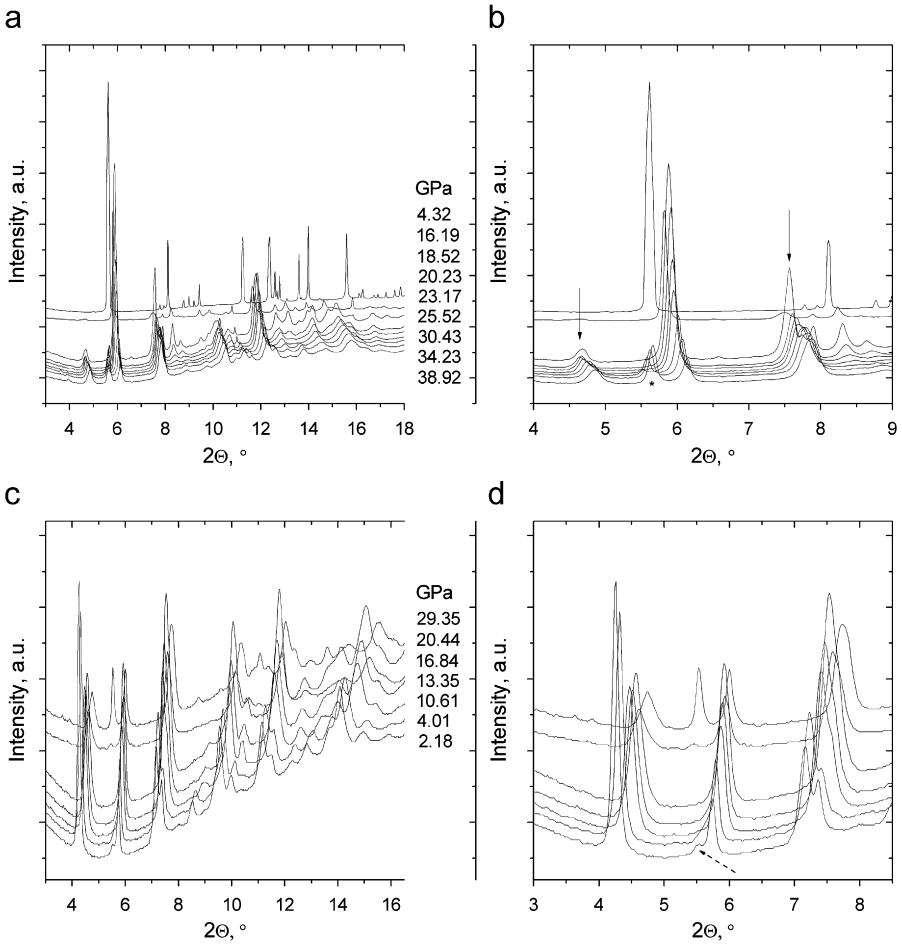

Fig. 2. Synchrotron X-ray diffraction patterns of $NaZnF_3$ acquired on compression ((a), detailed fragment (b)) and decompression ((c), detailed fragment (d)). Arrows (in (b)) mark main features corresponding to postperovskite $NaZnF_3$ phase; asterisk marks peak corresponding to high-pressure modification (see text). Dashed arrow (in (d)) indicate peak of the incipient $NaZnF_3$ perovskite.

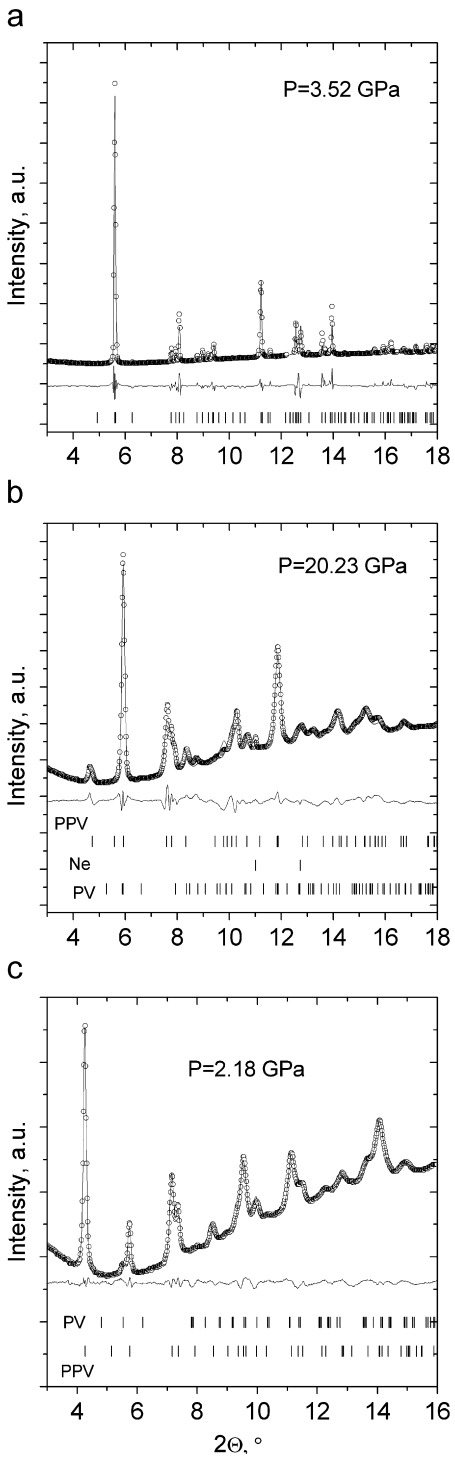

Fig. 3. Examples of the results of Rietveld refinement corresponding to 3.52 GPa on the compression (a) ($R_p = 0.03$, $wR_p = 0.06$), 20.23 GPa on the compression (b) ($R_p = 0.017$, $wR_p = 0.024$), and 2.18 GPa on the decompression (c) ($R_p = 0.0065$, $wR_p = 0.0083$).

3. Results and discussion

Fig. 1 shows the results of total energy calculations performed for perovskite and postperovskite modifications of $NaZnF_3$. At ambient pressure, as expected, perovskite phase is more stable than postperovskite. Above 25.4 GPa, DFT predicts higher thermodynamical stability of the postperovskite modification.

Fig. 2 represents XRD spectra obtained for $NaZnF_3$ on compression (a, b) and decompression (c, d), (not all observed spectra are given to keep the graphs distinct). Systematic shift of the peaks is due to progressive lattice contraction with increasing pressure. We must note further that above approximately 14 GPa, sharp reflections transform into rather broad peaks. This process is accompanied by significant reduction of the peak intensity and found to be irreversible. One of the possible explanations for the phenomenon is the onset of pressure-induced amorphization and/or introduction of the structural distortion. It is more likely, however, that this effect is attributed to the grain decomposition due to the reconstructive phase transition. Indeed, another phenomenon observed at this pressure (14 GPa) is an appearance of additional features in the spectra (marked with arrows in Fig. 2b). These peaks were ascribed to the incipient postperovskite phase. Correctness of the assumption is supported with fairly good quality of the Rietveld fit for multiphase model (see below). It must be noted that pv→ppv phase transition in $NaZnF_3$ occurs in rather wide pressure range: from 14 to 22 GPa. For comparison, $NaMgF_3$ transforms to $CaIrO_3$ postperovskite structure in the pressure range from 28 to 30 GPa [6]. Increasing pressure above 25 GPa resulted in appearance of additional reflections (marked with an asterisk in Fig. 2b) inconsistent with *Cmcm* space group of $CaIrO_3$ type. This phase transition is found to be fully reversible. Due to rather low quality of high-pressure X-ray diffraction data, attempts to identify this phase were fruitless. For this reason, acceptable Rietveld refinement was obtained for the pressures below 25 GPa. Post-postperovskite transitions were already reported for other studied compounds. For instance, Martin et al. [6] observed transformation of the postperovskite $NaMgF_3$ phase into unknown phase, presumably orthorhombic *Pnnm* (called by authors N-phase) at high pressure on laser heating. This phase is unstable and becomes X-ray amorphous upon decompression. Later, Tschauner et al. [15] proposed formation of kinked polymorphs of $CaIrO_3$ type that could explain inconsistency between *Cmcm* $CaIrO_3$ model and high-pressure X-ray diffraction data. Further data analysis is in progress.

Another important peculiarity of high-pressure structural behavior of $NaZnF_3$ is high stability of ppv phase on decompression. As can be seen from the data presented in Figs. 2c and d, the sample retains postperovskite structure down to 2.18 GPa (the lowest pressure achieved in this experiment on decompression). At 2.18 GPa only feebly marked peak from the incipient pv phase is observed (indicated with dashed arrow in Fig. 2d). As energy minimization calculations with VASP resulted in lower total energy for pv structure at near-ambient pressures, we assume that observed low-pressure ppv phase is metastable and reverse ppv→pv phase transition is kinetically hindered at ambient temperature. This hysteresis in pv→ppv phase transition and very low pressure at which it occurs (the lowest reported) make $NaZnF_3$ a model object for studies of pressure-induced phase transformations in perovskite-type compounds. According to the literature, the pressures of pv→ppv phase transition reported for other perovskite compounds are very high (28–30 GPa for $NaMgF_3$ [6], above 60 GPa for $MnGeO_3$ [4] and $MgGeO_3$ [5] and above 100 GPa for $MgSiO_3$ [2,3]) and hence experiments and data analysis are far more complicated.

Fig. 3 shows the results of Rietveld refinement of data obtained at 3.52 and 20.23 GPa on compression (a, b) and 2.18 GPa after decompression (c). Table 1 summarizes the refined lattice parameters and unit cell volumes of pv and ppv modifications of $NaZnF_3$. At elevated pressure, poor overall data quality resulted in lower accuracy of the lattice parameters determination.

Fig. 4 represents fit of *P*–*V* data (observed (a) and ab-initio DFT calculated (b)) to the third-order Birch–Murnaghan equation of

Table 1
Lattice parameters and unit cell volumes of perovskite and postperovskite modifications of $NaZnF_3$.

P (Gpa)	a (Å)	b (Å)	c (Å)	V (Å^3)
Perovskite (*Pnma*)				
Compression				
0	5.5551±0.0001	7.7308±0.0002	5.3863±0.0001	231.37±0.01
3.52	5.5213±0.0008	7.6097±0.0026	5.3035±0.0005	222.83±0.08
4.32	5.5061±0.0006	7.6159±0.0021	5.2769±0.0008	221.28±0.06
7.68	5.4717±0.0006	7.5401±0.0009	5.2008±0.0006	214.57±0.03
8.93	5.4614±0.0006	7.5174±0.0007	5.1769±0.0006	212.54±0.03
11.35	5.4482±0.0008	7.4018±0.0029	5.1259±0.0007	206.71±0.09
12.90	5.4387±0.0012	7.3816±0.0022	5.0902±0.0011	204.35±0.06
14.30	5.4398±0.0017	7.3629±0.0029	5.0621±0.0017	202.75±0.14
16.19	5.4210±0.0022	7.3447±0.0043	5.0006±0.0020	199.10±0.08
17.34	5.4215±0.0021	7.3069±0.0020	4.9885±0.0023	197.62±0.12
18.52	5.4240±0.0043	7.2684±0.0016	4.9441±0.0102	194.92±0.36
20.23	5.3944±0.0066	7.2746±0.0131	4.8765±0.0051	191.36±0.32
21.95	5.3877±0.0079	7.2111±0.0210	4.8633±0.0059	188.94±0.54
23.17	5.3732±0.0094	7.2081±0.0233	4.8593±0.0106	188.20±0.29
Postperovskite (*Cmcm*)				
Compression				
18.52	2.9514±0.0025	9.1405±0.0169	7.2362±0.0091	195.21±0.18
20.23	2.8885±0.0014	9.0720±0.0064	7.2120±0.0041	188.99±0.09
21.95	2.8884±0.0015	9.0234±0.0066	7.1782±0.0039	187.08±0.09
23.17	2.8828±0.0014	9.0104±0.0061	7.1575±0.0037	185.92±0.09
24.40	2.8732±0.0014	9.0365±0.0050	7.1099±0.0033	184.60±0.10
Decompression				
20.44	2.8857±0.0010	9.1136±0.0038	7.1411±0.0026	187.81±0.18
16.84	2.9030±0.0010	9.2320±0.0036	7.1684±0.0023	192.12±0.16
15.39	2.9122±0.0010	9.2755±0.0037	7.1893±0.0024	194.20±0.17
14.43	2.9185±0.0009	9.3217±0.0036	7.2043±0.0022	195.99±0.16
13.35	2.9244±0.0009	9.3699±0.0036	7.2170±0.0021	197.75±0.15
12.47	2.9310±0.0008	9.4075±0.0034	7.2311±0.0020	199.39±0.15
11.52	2.9362±0.0006	9.4446±0.0027	7.2413±0.0015	200.81±0.11
10.61	2.9424±0.0008	9.4846±0.0034	7.2545±0.0019	202.45±0.14
9.46	2.9532±0.0008	9.5409±0.0033	7.2758±0.0018	205.01±0.14
4.01	3.0016±0.0007	9.8647±0.0033	7.3836±0.0017	218.63±0.14
2.18	3.0335±0.0007	10.0316±0.0034	7.4502±0.0018	226.71±0.14

state. Table 2 summarizes $K_{P,0}$, $K'_{P,0}$, V_0 (equilibrium cell volume) and R^2 (squared correlation factor of the fit). In the case of the experimental data, first derivatives of bulk moduli were fixed at 4. One can see that first-principles calculations resulted in noticeably higher bulk modulus, $K_{P,0}$, and lower fitted unit cell volume for both pv and ppv phases. However, despite the inaccuracy, in absolute values, DFT predicted higher bulk modulus for ppv phase (Table 2). Experimentally obtained $K_{P,0}$ of perovskite $NaZnF_3$ is slightly lower than the value reported for perovskite $NaMgF_3$ by Martin et al. [6] (76.5 GPa) and several times lower than those known for oxide perovskites. This low $K_{P,0}$ of pv $NaZnF_3$ is consistent with its relative instability. Very important distinction of $NaZnF_3$ from $NaMgF_3$ is that pv and ppv modifications of $NaZnF_3$ are characterized by very close values of $K_{P,0}$ (Table 2). Yet, bulk modulus of ppv $NaMgF_3$ is about two times higher (137±18 GPa, [6]) than that of pv. In the case of $NaZnF_3$, similar elastic properties of pv and ppv modifications can explain rather broad pressure range of phase transition.

Pressure-dependent reduced lattice parameters obtained for pv (a) and ppv (b) phases on compression and decompression, respectively, are shown in Fig. 5. For ppv phase, lattice parameters corresponding to 2.18 GPa were used as a reference. Both pv and ppv phases are characterized by highly anisotropic compressibilities. It is important to notice that, in the case of ppv phase, the highest compressibility was found for the direction of b axis, i.e. perpendicular to the layers of ZnF_6 octahedra arrangement in $CaIrO_3$-type structure. These results are in a complete agreement with earlier report by Hirose et al. [5] on $MgGeO_3$ postperovskite.

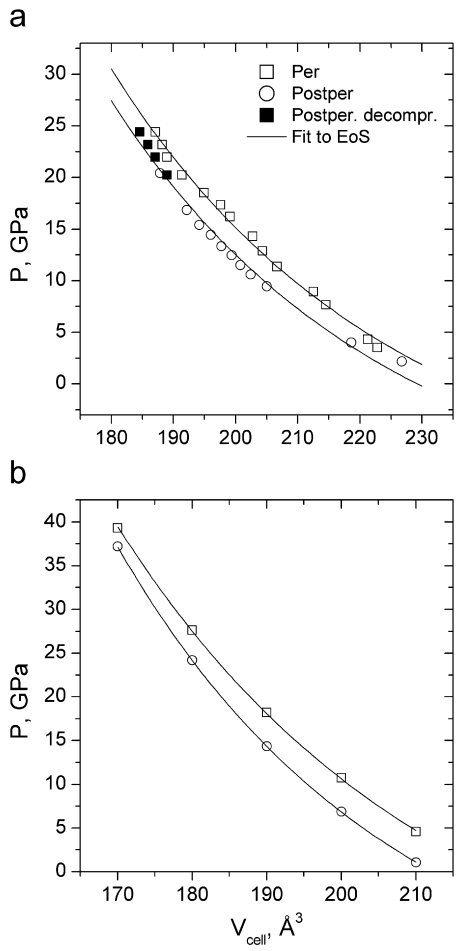

Fig. 4. Fit to the third order Birch–Murnaghan equation of state (solid line) of P–V data obtained from high-pressure X-ray diffraction data (a) and DFT ab-initio calculation (b) (markers).

Table 2
Bulk moduli and parameters of fit of P–V data (ab-initio DFT simulation and experiment) to third-order Birch–Murnaghan equation of state.

	DFT		Experiment	
	pv	ppv	pv	ppv
$K_{P,0}$ (GPa)	92.93±2.95	100.26±0.25	64.98±2.67	69.88±3.69
$K'_{P,0}$	3.89±0.12	4.59±0.01	4 (fixed)	
$V_{0,cell}$ (Å^3)	219.96±0.54	212.28±0.03	236.31±1.28	229.23±1.53
R^2	1	1	0.994	0.988

4. Summary

To conclude, crystallochemical approach was used to select perovskite compound ($NaZnF_3$) for which perovskite–postperovskite phase transition can potentially be observed. High-pressure structural behavior of $NaZnF_3$ was investigated by means of first-principles computations and monochromatic synchrotron X-ray powder diffraction. With increasing pressure, perovskite phase gradually transforms into postperovskite in the pressure range 14–22 GPa. This is the lowest pressure reported for pv→ppv transition. Above 25 GPa, ppv structure coexists with another phase, presumably high-pressure polymorph of $CaIrO_3$ structural type. On decompression, pure ppv phase was found to be stable down to 4 GPa. This hysteresis was attributed to kinetic hindrance

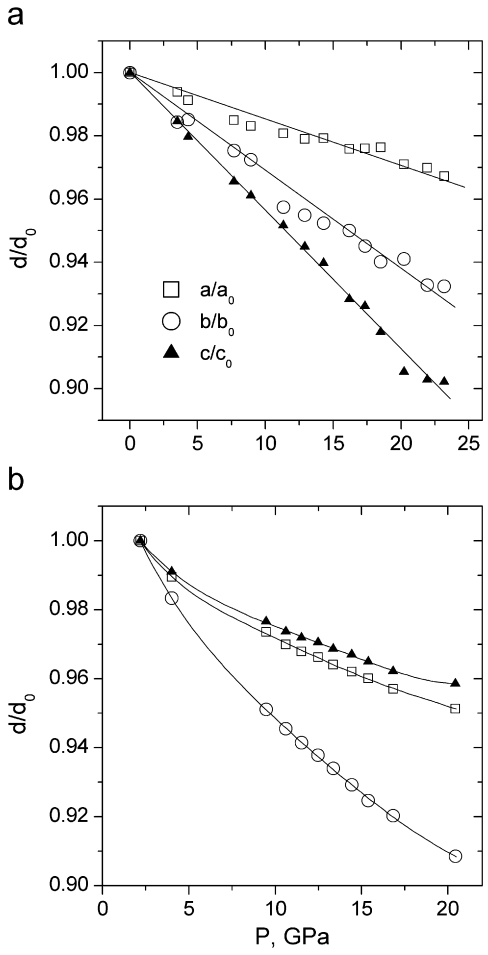

Fig. 5. Reduced lattice parameters of perovskite (a) and postperovskite (b) obtained for $NaZnF_3$ on compression and decompression, respectively. Solid lines are the guide for the eye only.

of reverse ppv→pv transformation. Bulk moduli obtained from fit of observed *P–V* data are 64.98 ± 2.67 GPa (for pv) and 69.88 ± 3.69 GPa (for ppv). Both pv and ppv modifications of $NaZnF_3$ are characterized by significant anisotropy of compression. For ppv, the most compressible direction is perpendicular to planes of ordering of ZnF_6 octahedra.

Acknowledgments

The authors thank Dr. G. Garbarino and Dr. W.A. Crichton (ID27, ESRF) for the help with high pressure DAC experiment and the Australian Partnership for Advanced Computing (APAC) for allocation of supercomputer time.

References

[1] L.G. Tejuka, J.L.G. Fierro, Properties and Applications of Perovskite-type Oxides, Marcel Dekker, New York, 1993.
[2] M. Murakami, K. Hirose, K. Kawamura, N. Sata, Y. Ohishi, Science 304 (2004) 855–858.
[3] S. Ono, A.R. Oganov, Earth Planet. Sci. Lett. 236 (2005) 914–932.
[4] S. Tateno, K. Hirose, N. Sata, Y. Ohishi, Phys. Chem. Miner. 32 (2006) 721–725.
[5] K. Hirose, K. Kawamura, Y. Ohishi, S. Tateno, N. Sata, Am. Miner. 90 (2005) 262.
[6] C.D. Martin, W.A. Crichton, H. Liu, V. Prakapenka, Geophys. Res. Lett. 33 (2006) L11305.
[7] M. Mezouar, W.A. Crichton, S. Bauchau, F. Thurel, H. Witsch, F. Torrecillas, G. Blattmann, P. Marion, Y. Dabin, J. Chavanne, O. Hignette, C. Morawe, C. Borel, J. Synch. Radiat. 12 (2005) 659–664.
[8] I.N. Goncharenko, High Press. Res. 27 (2007) 183–188.
[9] M. Avdeev, E.N. Caspi, S. Yakovlev, Acta Cryst. B 63 (2007) 363–372.
[10] H.K. Mao, J. Xu, P.M. Bell, J. Geophys. Res. 91 (1986) 4673–4676.
[11] A.P. Hammersley, S.O. Svensson, M. Hanfland, A.N. Fitch, D. Hauserman, High Pressure Res. 14 (1996) 235–248.
[12] B.H. Toby, J. Appl. Cryst. 34 (2001) 210–213.
[13] A.C. Larson, R.B. Von Dreele, General structure analysis sysgem (GSAS), Los Alamos National Laboratory Report LAUR 86–748, 2004.
[14] J. Hafner, Comput. Phys. Commun. 177 (2007) 6–13.
[15] O. Tschauner, B. Kiefer, H. Liu, S. Sinogeikin, M. Somayazulu, S.-N. Luo, Am. Miner. 93 (2008) 533–539.